Water **2015**, *7*, 4385-4408; doi:10.3390/w7084385

OPEN ACCESS

water

ISSN 2073-4441

www.mdpi.com/journal/water

Article

Fractal Dimension of Cohesive Sediment Flocs at Steady State under Seven Shear Flow Conditions

Zhongfan Zhu [1], Jingshan Yu [1], Hongrui Wang [1,*], Jie Dou [2] and Cheng Wang [3]

[1] College of Water Sciences, Beijing Normal University, Xinjiekouwai Street 19, Beijing 100875, China; E-Mails: zhuzhongfan1985@gmail.com (Z.Z.); jingshan@bnu.edu.cn (J.Y.)

[2] Department of Natural Environmental Studies, The University of Tokyo, Kashiwa 277-8568, Japan; E-Mail: douj888@gmail.com

[3] Environmental Science Division, Argonne National Laboratory, Lemont, IL 60439, USA; E-Mail: chengw@knights.ucf.edu

* Author to whom correspondence should be addressed; E-Mail: henrywang@bnu.edu.cn; Tel.: +86-10-5880-2736.

Academic Editor: Y. Jun Xu

Received: 11 May 2015 / Accepted: 5 August 2015 / Published: 12 August 2015

Abstract: The morphological properties of kaolin flocs were investigated in a Couette-flow experiment at the steady state under seven shear flow conditions (shear rates of 5.36, 9.17, 14, 24, 31, 41 and 53 s^{-1}). These properties include a one-dimensional (1-D) fractal dimension (D_1), a two-dimensional (2-D) fractal dimension (D_2), a perimeter-based fractal dimension (D_{pf}) and an aspect ratio (AR). They were calculated based on the projected area (A), equivalent size, perimeter (P) and length (L) of the major axis of the floc determined through sample observation and an image analysis system. The parameter D_2, which characterizes the relationship between the projected area and the length of the major axis using a power function, $A \propto L^{D_2}$, increased from 1.73 ± 0.03, 1.72 ± 0.03, and 1.75 ± 0.04 in the low shear rate group (G = 5.36, 9.17, and 14 s^{-1}) to 1.92 ± 0.03, 1.82 ± 0.02, 1.85 ± 0.02, and 1.81 ± 0.02 in the high shear rate group (24, 31, 41 and 53 s^{-1}), respectively. The parameter D_1 characterizes the relationship between the perimeter and length of the major axis by the function $P \propto L^{D_1}$ and decreased from 1.52 ± 0.02, 1.48 ± 0.02, 1.55 ± 0.02, and 1.63 ± 0.02 in the low shear group (5.36, 9.17, 14 and 24 s^{-1}) to 1.45 ± 0.02, 1.39 ± 0.02, and 1.39 ± 0.02 in the high shear group (31, 41 and 53 s^{-1}), respectively. The results indicate that with increasing shear rates, the flocs become less elongated and that their boundary lines become tighter and more regular, caused by more breakages and possible restructurings of

the flocs. The parameter D_{pf}, which is related to the perimeter and the projected area through the function $A \propto P^{2/D_{pf}}$, decreased as the shear rate increased almost linearly. The parameter *AR*, which is the ratio of the length of the major axis and equivalent diameter, decreased from 1.56, 1.59, 1.53 and 1.51 in the low shear rate group to 1.43, 1.47 and 1.48 in the high shear rate group. These changes in D_{pf} and *AR* show that the flocs become less convoluted and more symmetrical and that their boundaries become smoother and more regular in the high shear rate group than in the low shear rate group due to breakage and possible restructuring processes. To assess the effects of electrolyte and sediment concentration, 0.1 mol/L calcium chloride ($CaCl_2$) and initial sediment concentration from 7.87×10^{-5} to 1.57×10^{-5} were used in this preliminary study. The addition of electrolyte and increasing sediment concentration could produce more symmetrical flocs with less convoluted and simpler boundaries. In addition, some new information on the temporal variation of the median size of the flocs during the flocculation process is presented.

Keywords: flocculation; fractal dimension; cohesive sediment; steady state; shear flow

1. Introduction

When fine-grained sediment particles are transported in estuarine and coastal waters, they continually flocculate to form flocs of different sizes due to small-scale, particle–particle interactions. In addition, some flocs may break into smaller fragments/particles due to flow shear (breakup or disaggregation) [1,2–5], which results in flocs with varying sizes, excess densities and different setting velocities.

The concept of fractal geometry provides a useful mathematical framework for describing the structural properties of irregular objects [6]. For the fractal flocs formed in a water-sediment mixture, properties such as volume, mass and density should be scaled as a power of their characteristic size (the exponent has been termed a three-dimensional (3-D) fractal dimension).Thus, this fractal dimension is a measure of how primary particles fill the entire space of the floc. Similar to the 3-D fractal dimension, 2-D, 1-D and perimeter-based fractal dimensions have been defined and used to characterize the extent of the morphological irregularity of the floc boundary and/or its shape in the projected plane [7–9].

Most studies regarding shear-induced particle flocculation have been focused on two main aspects: (1) the time evolution of the size distribution and the structural and morphological properties of the flocs during the aggregation/coagulation/flocculation processes; and (2) investigations of the floc properties at the steady or equilibrium states, where the property parameters reach constant values.

The already reported experimental results on the temporal evolution of the size distribution of the flocs during the aggregation process exhibited two different trends. In the first trend, the median size distribution of the flocs rapidly increases with time at the beginning of flocculation development and then continually slows down until a steady state is approached [7–19]. This type of size-time profile is henceforth referred to as type I. However, the profile is referred to as type II when the median size initially increases to a maximum value with time and then decreases again before reaching a steady state [9,11,19–24]. This peak in the size-time curve during the aggregation process potentially occurs as

a result of breakups and/or restructurings (breakages and re-aggregations) of the flocs according to recent studies conducted by Bubakova *et al.* and Selomulya *et al.* [9,22].

In contrast to the floc size properties, we found that insufficient attention was paid to the morphological properties of the flocs at the steady state with respect to shear conditions. Thus, the main objective of this study is to investigate the dependency of the morphological properties of flocs on the shear conditions by analyzing the variations in the fractal dimensions of flocs at the steady state with respect to different shear stresses in a Couette-flow experimental system. Furthermore, the effects of adding the electrolyte and improving the sediment concentration on the steady-state floc properties are explored. In addition, this study supplements existing knowledge regarding the evolution of the size distribution of flocs during the flocculation process.

This paper is arranged as follows. First, the definitions of the three fractal dimensions and the aspect ratio used for characterizing the morphological properties of cohesive sediment flocs is introduced in Section 2. In addition, Section 2 briefly describes the methods used in this study, including the Couette-flow experiment system, a sampling procedure and an image-processing method. The fractal dimensions and aspect ratios under different shear conditions and the evolution of the floc size distribution with time during the shear-induced flocculation process are discussed in Section 3 which also describes the effect of electrolyte condition and presents an examination of the initial sediment concentration. Finally, two conclusions are drawn in Section 4.

2. Fractal Dimension and Experimental Setup

2.1. Fractal Dimension Analyses

For a floc that satisfies the self-similar law, the volume, V, is related to the characteristic length of the floc (this length has generally been regarded as the length of the major axis of the floc or the maximum length, L)as follows:

$$V \propto L^{D_3} \tag{1}$$

where D_3 is the 3-D fractal dimension, which varies from 1 to 3 and is defined to characterize the space-filling ability of the floc [8,25,26]. Similarly, the projected surface area, A, of the floc could be assumed to follow the power-law function for its maximum length as follows:

$$A \propto L^{D_2} \tag{2}$$

where D_2 is the 2-D fractal dimension defined for relating the characteristic length to the projected surface area in a projected plane [7,9,25,26]. For a perfectly spherical particle, D_2 equals to 2. Values for D_2 smaller than 2 indicate that the projected area increases more slowly than the Euclidean object of the same length when the maximum floc length increases (for which the value of D_2 is 2), and that the floc is elongated along the direction of its major axis. The more closely the value of D_2 approaches 2, the smaller the degree to which the floc is elongated.

Similar to Equation (2), Serra and Casamitjana [8] described a relationship between the perimeter, P, of a floc and its major axis length in terms of an additional fractal dimension, D_1, as follows:

$$P \propto L^{D_1} \tag{3}$$

where D_1 is the 1-D fractal dimension relating the major axis length to the perimeter in a projected plane [7]. For a spherical particle, D_1 equals to 1. Values of D_1 greater than 1 indicate that the perimeter increases more rapidly than the Euclidean perimeter when the maximum floc length increases by the same length (for which the value of D_1 is 1) and that the boundary line of the floc becomes loose and jagged. The closer the D_1 value is to 1, the tighter and more regular the boundary line of the floc becomes.

From Equations (1) and (2), the following simple relationship between the volume and the projected surface area can be obtained:

$$V \propto A^{D_3/D_2} \tag{4}$$

Similar to Equation (4), a simple relationship between the projected area and the perimeter could be quantified in terms of the perimeter-based fractal dimension, D_{pf}, as follows:

$$A \propto P^{2/D_{pf}} \tag{5}$$

where D_{pf} relates the perimeter to the projected surface area in a projected plane [7–9,27,28]. The value for D_{pf} is between 1 and 2, with the value of 1corresponding to a spherical floc and the value of 2 corresponding to a linear one. Values of D_{pf} greater than 1 indicate that the perimeter increases more rapidly than the Euclidean perimeter as the projected area of the floc increases across the projected plane for which the D_{pf} value is 1. As a result, the floc boundary becomes more convoluted and scraggier and has a more irregular shape. When the value of D_{pf} is approximately 2, the extent by which the boundary of the floc becomes convoluted is more serious.

The aspect ratio (AR), the ratio of the major axis length and equivalent size (or diameter), L_e, is defined as follows:

$$AR = L/L_e \tag{6}$$

where L_e is the diameter of a circle whose enclosed area is equivalent to the projected surface area. A small AR value near 1 results from a floc with a symmetrical shape.

2.2. Experiment Description

2.2.1. Turbulence-Generating Device

Among various systems that could be used to generate a shear flow, such as an impeller mixer, an oscillating grid and the Couette apparatus [9,12,14,27,29], the Couette-flow system was used in this study because it can generate a more isotropic shear flow than any other devices and avoids the need to account for the impacts of turbulence heterogeneity on the flocculation process [18,23,30]. The Couette device consists of an inner cylinder with a radius of 150 mm and an outer cylinder with a radius of 236 mm and 682 mm tall. The outer cylinder was fixed and the inner cylinder was rotated at different angular speeds to create a shear flow between the cylinders where flocculation occurs. Both cylinders were made of Plexiglas to allow the suspension to be visible. The angular velocities of the inner cylinder were controlled by a speed-adjusting motor (angular velocity ranges from 108 to 1350 revolutions per minute (rpm); it is a 180 Watt three-phase induction motor, produced by the Beijing Orient Drive Industry Corporation, China) coupled with three different-sized speed reduction boxes (with speed

reduction ratios of 180, 25 and 7.5 respectively, and produced by the Beijing Orient Drive Industry Corporation in China), thereby ranging from 1.8 to 180 rpm.

2.2.2. Shear Rate Calculation

In most shear-induced flocculation experiments, the shear rate (or the shear velocity gradient), *G*, has been used to characterize the shear flow [10,12,14,23,27,30,31]. This parameter was determined using two different methods, depending on whether the flow is laminar or turbulent. For laminar flow, the shear rate, *G*, is the average value of the gradient of the tangential velocity along the axial direction across the gap of the cylinders in the cylindrical coordinate system. The shear rate was calculated to estimate the mean shear by using the following expression [10,12,29]:

$$G = \frac{2\omega R_1 R_2}{R_2^2 - R_1^2} \tag{7}$$

where ω is the angular velocity of the inner cylinder and R_1 and R_2 are the radii of the inner and outer cylinders, respectively. For turbulent flow, the *G* value was determined as follows [1,14,32,33]:

$$G = \sqrt{\frac{\varepsilon}{\nu}} \tag{8}$$

where ε is the energy dissipation rate per unit mass (m^2/s^3) and υ is the kinematic viscosity of the fluid (m^2/s). Because the *G* value is estimated using different expressions (Equations (7) and (8)), the critical angular velocity at which the transition of the shear flow from the laminar state to the turbulent state, ω_c, should be evaluated before calculating the *G* value. An acoustic doppler velocity-meter (ADV) (with velocity ranges from 1 mm/s to 2.5 m/s, and accuracy 0.1 mm/s with a standard deviation of 1%; produced by SonTek Corporation, San Diego, CA, USA) was used to measure the flow field in the Couette-flow system as the angular velocity of the inner cylinder was increased. Three ADV probes, each 38.5 mm in length, were used to measure the radial, tangential and vertical components of the velocity, respectively. Due to the limitations of the relative ADV dimensions and the Couette-flow system in the present experiment, only the velocities of some points along the vertical direction in the center of the gap of the cylinders can be detected (the number of measured points was 8~9 and they were evenly distributed along the vertical direction in this experiment). By using spectrum analysis of the measured velocity data [34], the critical angular velocity of the inner cylinder at which the transition to turbulence occurs was found to be ω_c = 27 rpm (a detailed description can be found in Zhu [35]). To avoid discussing the effects of too many shear rates on the flocculation process and for technical reasons, the angular velocities of the inner cylinder were set at 24, 42, 60, 90, 120, 150 and 180 rpm to cover the transition from laminar to turbulent flow. The exact value for the rate of the energy dissipated into the system, ε, is difficult to estimate, and in the present study, we used the method presented by Serra *et al.* [12]. In this method, ε is assumed to scale according to $\varepsilon \propto u'^3/\ell$ when using a characteristic velocity fluctuation, u', and a characteristic length, ℓ. It was further assumed that the value of ℓ is scaled to the width of the gap, $\ell \propto R_2 - R_1$. Here it seems much more reasonable to use the averaged velocity fluctuation measured by ADV, $\overline{u'}$, to replace the value of u'. This method was used instead of the method of Serra *et al.* where the value of u' was simply assumed to scale to the mean velocity,

which was a specific function of the angular velocity of the inner cylinder (see Equation (8) in Serra *et al.*) [12]. However, if continuity between the laminar shear rate and the turbulent shear rate at the critical angular velocity ω_c is assumed, a proportionality ratio, p, can be obtained. The shear rate values corresponding to different angular velocities of the inner cylinder exceeding the critical value can finally be calculated if the p value is determined. Here, Equation (8), together with these scaling relationships, provides an approximate estimation of the shear rate value and is only used as a basis for comparing various shear rate effects of the flocculation process. In this study, the p value was $p = 1.65 \times 10^{-3}$, which is smaller than the value ($p = 0.03$) obtained by Serra *et al.* and others when studying naturally turbulent systems (e.g., $p = 0.37$ in Lazier and Mann and $p = 0.50$ in Bower *et al.*) [12,36,37]. Table 1 presents the calculated shear rates that correspond to all of the angular velocities of the inner cylinder used in the present study (as presented in the third row in Table 1) and the measured averaged velocity fluctuation values (as presented in the second row in Table 1). The shear rate value clearly increases as the angular velocity of the inner cylinder increases, ranging from 5.36 to 53 s^{-1}; the shear rate corresponding to the critical value of the angular velocity of the inner cylinder is 5.96 s^{-1}. In some natural open systems, typical values of G are between 0.3 and 10 s^{-1} in coastal zones, 0.1 and 400 s^{-1} in near shore lake zones, and 0 and 35 s^{-1} in estuarine areas [38–42]. However, for engineered water treatment systems, typical values of 20 to 50 s^{-1} are generally used in horizontal shaft turbines and values of 10 to 80 s^{-1} are generally used in vertical shaft turbines [29,43]. Therefore, the shear rate values used in this study could represent the shear conditions in reality and the findings of this study could be a reference for research on particle flocculation/coagulation in natural shear environments and/or water treatment environmental conditions. The flow between the cylinders becomes unstable as long as the angular velocity of the inner cylinder is larger than a certain value [44].

$$\omega_i = \nu \sqrt{\frac{3390\left(R_2^2 - R_1^2\right)}{4R_1^2\left(R_2 - R_1\right)^4}} \tag{9}$$

In our case, $\omega_i = 0.05$ s^{-1} (0.5 rpm). The Taylor vortices due to flow instability were observed during all the experimental runs because all the angular velocity values of the inner cylinder in this study exceeded this ω_i value.

Table 1. Shear flow parameters with respect to different angular velocities of the inner cylinder.

ω (rpm)	**24**	**27**	**42**	**60**	**90**	**120**	**150**	**180**
$\overline{u'}$ (mm/s)	0	0	31.5	39.1	57.6	70.8	81.5	103.2
G (s^{-1})	5.36	5.96	9.17	14	24	31	41	53
Pe	406	452	695	1062	1820	2352	3110	4021

2.2.3. Sediment

To avoid estimating the effects of several mineral compositions on the flocculation process, kaolin (China clay) was used in this experiment because of its obvious flocculation characteristics, as described in many previous experiments [23,45–48]. The particle size distribution of the kaolin was determined using

a laser particle size analyzer (Horiba LA-920; produced by Horiba Corporation, Tokyo, Japan). The measured size distribution is plotted in Figure 1, and the distribution statistics are provided in Table 2.

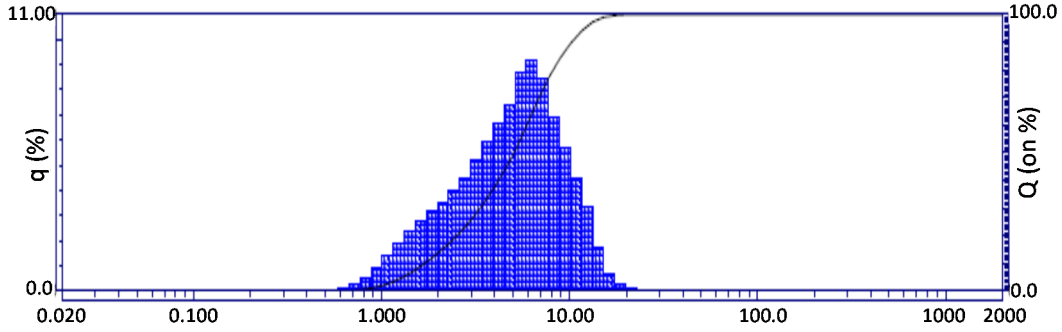

Figure 1. Particle size distribution of the kaolin. The left vertical axis (corresponding to blue bars) and the right one (corresponding to the black curve) denote the individual and cumulative percentile of different-sized particles over the total, respectively, whereas the longitudinal axis represents different size values (the unit is micron).

Table 2. Particle-size distribution statistics for the kaolin.

Sediment	Range (μm)	d_{10} (μm)	d_{30} (μm)	d_{50} (μm)	d_{70} (μm)	d_{90} (μm)
Primary particles	0.59~23	1.7	3.36	5.07	6.89	10.27

2.2.4. Experimental Procedure

A schematic view of the experimental procedure is shown in Figure 2a. Specified amounts of deionized water were poured into the region between the cylinders for each experimental run to ensure that the height of the water-sediment mixture is kept at approximately 400 mm during the experiments (in view of the super-elevation of the surface of the mixture that resulted from eccentric motion and the benefits of the sampling operations). A specific amount of kaolin sediment by volume fraction was added to the mixture, $\phi = 7.87 \times 10^{-5}$, and introduced into the Couette-flow system before adjusting the annular velocity of the inner cylinder to its maximum value for five minutes to guarantee that the kaolin was adequately suspended in the system. Compressed nitrogen gas (N_2) was released into the water-sediment mixture from a circular hole with a diameter of 40 mm at the bottom of the outer cylinder to yield a strong impulse for dispersing the suspension so that no flocs of primary kaolin particle were present before initiating the experiment. At the beginning of the experimental run, the specified shear rate was rapidly reached by setting the rotation velocity of the inner cylinder using the speed-adjusting motor and the speed reduction boxes. By using a glass transfer pipette with a diameter of 5 mm [38,49], a water-sediment sample with approximate 1 mL volume was removed from a middle point in the vertical direction in the center of the gap between the outer and inner cylinders, where the velocity was measured by the ADV. By gently sloping the transfer pipette, the collected 0.1 mL sample (approximately two drops) was only allowed to fall out of the pipette into a small, glass volumetric flask with 1 mL deionized water to dilute it by its own weight instead of releasing the entire sample from the pipette. This dilution process was determined using a series of pre-arranged experiments to guarantee that overcrowding of the flocs in each sample did not occur so that the floc properties could be measured. Before the sample was transferred from the pipette to the flask, the pipette was immersed below the

surface of the water in the flask, which minimized the impacts of the floc sedimentation process and the inertial effects that could yield plunging plumes of sediment when the transfer process was conducted abruptly [38]. After the dilution process was completed, a dropper with a glass head and a rubber end was used to draw a portion of the diluted 0.1 mL sample (almost two drops) from the flask and carefully return it to the circular concave trough of a glass slide with a cover glass for microscopic observation. New flocs did not result from the Brownian motion and a differential settling in the flask because the Brownian motion is only important for particles smaller than 1 micron [12,26]. Moreover, the depth of water in the flask was too small to provide enough space for significant differential settling. A biological fluorescence microscope connected to a high resolution CCD (Olympus DP 71, produced by Olympus Corporation, Japan) was used to take photographs of the sample. The camera system consisted of a 1360 × 1024 pixel progressive scanner with a 2/3 inch colorful CCD camera fitted with a 4× primary magnification objective lens, and can collect the image at 15 frames per second. The ratio of the pixel length to the physical length in the collected images was 1:1.25 microns, and the minimum detectable particle size was set to a pixel area of 1 × 1. Figure 2b presents an example that includes four typical flocs formed for $G = 5.36\ s^{-1}$ and $\phi = 7.87 \times 10^{-5}$ with an experimental time of 360 min without any salinity added into the suspension. All of the images were saved in a personal computer, and after careful thresholding, the morphological property parameters of the flocs presented in these images (such as the projected surface area, the perimeter, the equivalent size and the length of the major axis) were calculated by means of the Matlab software (Matlabversion7.0.0.19920 (R14), produced by MathWorks Corporation, Natick, MA, USA). For each shear condition, two samples were collected at the same sampling point, and for every sample, approximately thirty individual images were taken so that the same flocs were not counted more than once. Consequently, a minimum of 500 flocs was counted when determining the morphological property parameters. The three fractal dimensions were calculated from the slopes of the log−log based regression lines of the relevant parameters based on Equations (2), (3) and (5). The standard errors were applied in their determinations. Figure 3 illustrate the procedure for determining the fractal dimensions of all flocs as an example. These flocs were formed for $G = 14\ s^{-1}$ with $\phi = 7.87 \times 10^{-5}$ for 160 min (steady state). The value of AR was obtained by averaging all of the flocs using Equation (6). Additionally D_3 cannot be determined using the image processing system in this study because all of the obtained images were only projected on a two-dimensional plane.

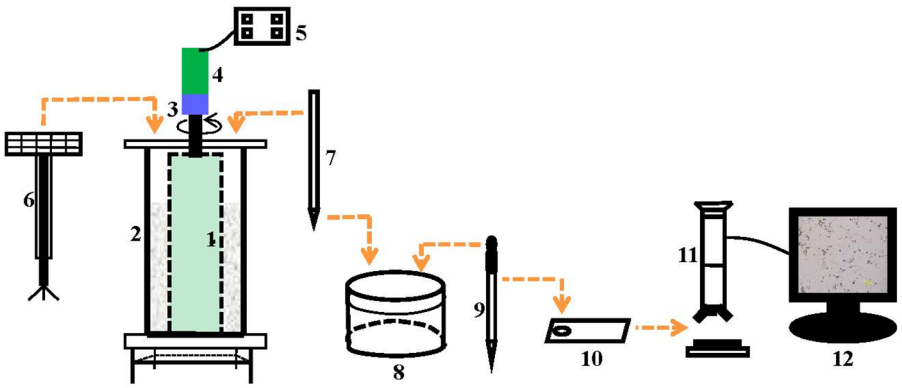

(a)

Figure 2. *Cont.*

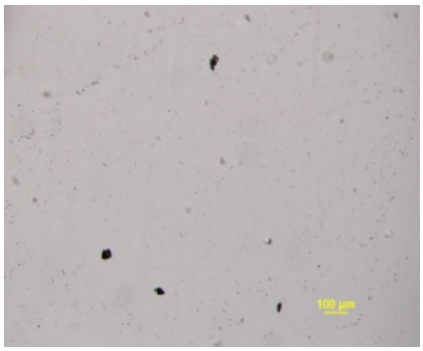

(**b**)

Figure 2. Schematic of the experimental setup (**a**) (1-the inner cylinder, 2-the outer cylinder, 3-a speed reduction box, 4-speed-adjusting motor, 5-a speed controller, 6-ADV, 7-a transfer pipette, 8-a volumetric flask, 9-a dropper, 10-a slide glass with a cover glass, 11-a biological fluorescence microscope connected to a high resolution CCD, and 12-an image processing system in the computer), and a representative example image (**b**) including four typical flocs, formed for G = 5.36 s^{-1} and ϕ = 7.87 × 10^{-5} at a experimental time of 360 min without electrolyte added into the suspension.

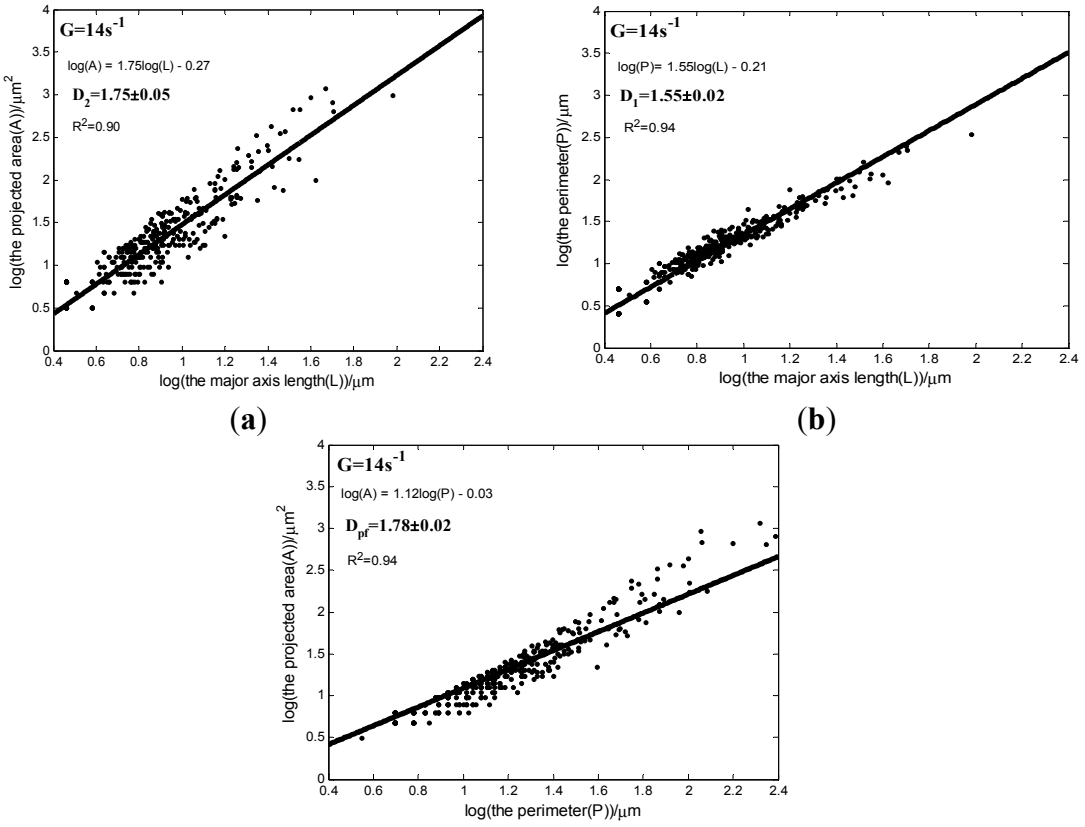

Figure 3. Determinations of 2-D (**a**), 1-D (**b**) and perimeter-based (**c**) fractal dimensions of the flocs as a representative example, which were formed for G = 14 s^{-1} and ϕ = 7.87 × 10^{-5} at a time of 160 min (steady state) without electrolyte added into the suspension, based on measurement data of major axis length, the perimeter and the projected surface area of the flocs using the image processing system.

Flocculation is governed by three dynamic mechanisms [1,5,32,50]: the Brownian motion, a differential settling and the fluid shear. The relative importance of the viscous force and the thermal force was quantified in terms of the Peclet number [8,10,12] as follows:

$$Pe = \frac{3\pi\eta G d_{50}^3}{4KT} \tag{10}$$

where η is the dynamic viscosity of the fluid (water in the present study), K is the Boltzmann constant and T is the temperature (as set at 20 ± 0.5 °C in all experiments). In the present experiment, the Peclet number varied from 406 to 4021 (as presented in the last row of Table 1). Thus, the flocculation due to the Brownian motion could be ignored relative to the shear-induced flocculation [10,12]. By performing experiments in a settling column, Stolzenbach and Elimelich [51] showed that the impact of the differential settling on the flocculation process in a dynamic marine environment was much smaller than that predicted using the theoretical collision function and could be negligible in many real situations. This conclusion has been acknowledged in several studies [1,32,52,53]. In our study, the effect of differential settling on flocculation development could be regarded as negligible because the shear stress values of a relatively large range were adopted in our experiment. No significant sediment deposition at the bottom of the outer cylinder was observed during all the experimental runs.

3. Results and Discussions

3.1. Attainment of Steady-State Flocculation Development

Figure 4 shows the evolution of the non-dimensional median floc size (or diameter), d_{50}^*/d_{50}, with the non-dimensional flocculation time, t^*, for shear conditions of G = 5.36, 14, 24, 31, and 53 s^{-1} respectively. Here, d_{50}^* is the median of the size distribution of the flocs formed in the shear flow and t^* depends on the shear rate G and on the primary sediment concentration ϕ as $t^* = tG\phi$ (where t is the flocculation time) because the non-dimensional parameter, tG, also known as the Camp number, is a design parameter for flocculation unit in water treatment engineering [3] and the non-dimensional time, $tG\phi$, denotes a normalized number of collisions among primary particles in the flow [8,10,12,31].

For the case G = 5.36 s^{-1}, the shear flow increases the collision frequency among primary particles at the beginning of the experiment according to the Smoluchowski equation [54] and, consequently, some large flocs are formed in the suspension, yielding a rapid increase of the median of the floc size distribution ($0 < t^* < 3$). These flocs have porous and fragile structures and are susceptible to breakage by the flow shear after a certain time, which makes the speed at which the median size increases with time gradually decrease ($3 < t^* < 6$). After a longer period, the breakage effect becomes much more pronounced until it balances the aggregation effect and, consequently, a steady-state floc size distribution is reached ($t^* > 6$). This behavior of the variation of the median size with respect to time describes the flocculation process of type I, which includes three phases: fast floc growth, slow floc growth and a steady state, as already introduced in Section 1 of this paper. A similar method for classifying these phases has been used by Keyvani and Strom who studied the influence of cycles of high and low turbulent shear on the growth processes of mud flocs [19].

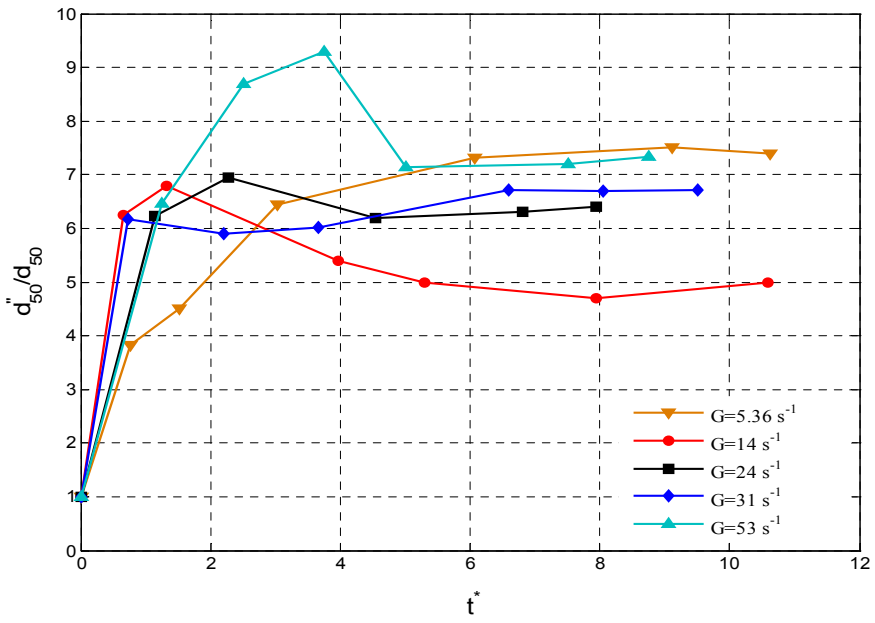

Figure 4. Evolution of the non-dimensional median flocsize of the flocs d_{50}^{*}/d_{50} with the non-dimensional flocculation time t^{*} for different shear rates at $\phi = 7.87 \times 10^{-5}$ without electrolyte added into the suspension.

In contrast, for shear cases of G = 14, 24, and 53 s^{-1}, the median floc size first increased with time to a maximum value during the early stage of flocculation development ($0 < t^{*} < 1.7$ for G = 14 s^{-1}, $0 < t^{*} < 2.1$ for G = 24 s^{-1}, and $0 < t^{*} < 3.7$ for G = 53 s^{-1}, respectively); as the flow shear increased, the collision frequency of primary particles and large and porous flocs were produced in the flow, and then decreased with time ($1.7 < t^{*} < 5$ for G = 14 s^{-1}, $2.1 < t^{*} < 4.5$ for G = 24 s^{-1}, and $3.7 < t^{*} < 5$ for G = 53 s^{-1}, respectively). This behavior potentially resulted from the strong breakages and restructurings of the fragile flocs when they were exposed to high shear stresses [9,20,22] before finally approaching a steady state due to the dynamic balance between fragmentation and re-aggregation after a long period ($t^{*} > 5$ for G = 14 s^{-1}, $t^{*} > 4.5$ for G = 24 s^{-1}, and $t^{*} > 5$ for G = 53 s^{-1}, respectively). This median size *vs.* time behavior depicts the flocculation process of type II, which is also composed of the three following phases: fast floc growth (referred to as type II-phase 1 herein), breakage and restructuring (type II-phase 2), and a steady state (type II-phase 3), as described in Section 1 of this paper. The type II-phase 1 presented in the figure could be approximately described as a simple linear increase process, as shown in several previous studies [9,11,20,21,55], rather than the exponential process reported by many authors [10,18,20,56]. Ehrl *et al.* [17] attributed the difference between the linear and exponential trends of the fast aggregate growth phase to different particle sizes for which the relative importance of Brownian motion and shear-induced aggregations changed correspondingly [9]. In this phase, the rate, λ, of the increase of the median floc size for different shear rates can be estimated using the following expression:

$$\lambda = \frac{\left(d_{50}^{''}\right)_{peak} - d_{50}}{\Delta t} \tag{11}$$

where $\left(d_{50}^{''}\right)_{peak}$ is the maximum value reached by the $d_{50}^{''}$, and Δt is the time period over which the $d_{50}^{''}$ increases from the primary value d_{50} (= 5.07 μm, see Table 2) to the peak value. The λ values are found

from Equation (11) to be 1.14, 1.63 and 2.84 μm/min for G = 14, 24 and 53 s^{-1} respectively. Thus, higher shear rates correspond with faster increases of the median floc size. This phenomenon does not agree with the experimental results reported by some researchers [9,10,22,57], probably because the collision efficiency improves with decreasing shear rates despite the lower collision frequency. However, our interpretation is as follows. According to the original Smoluchowski equation [54] (see also Equations (2) and (6) in Thomas *et al.* [3]), which is applicable to the fast floc growth phase because the breakage effect does not play a significant role in this stage, the rate of flocculation, k_{ij}, between the particles/flocs of sizes i and j is proportional to the collision efficiency α and the collision frequency, β_{ij}, between them and to the product of their respective number concentrations, n_i and n_j, as described in the following expression:

$$k_{ij} = \alpha\beta_{ij}n_i n_j \tag{12}$$

The collision efficiency factor, α, greatly depends on the effects of all short-range forces between two colliding particles/flocs [3], such as van der Waals attractive forces and double-layer electrostatic repulsive forces, and is thus a function of the surface physico-chemical characteristics of the sediment particle and water and the organic and inorganic compounds in the particle (no such substances here) [1]. For a given flocculation environment in this study, this factor can be simply regarded as a constant. Since the collision frequency function, β_{ij}, between the particles/flocs of sizes i and j is directly proportional to the shear rate, G [54] (see also Equation (6) in Thomas *et al.* [3]), a higher shear rate results in more collisions between particles/flocs. Consequently, the flocculation rate becomes larger and the median floc size increases more rapidly at a higher shear rate. Additionally, the local extreme value of d_{50} given G = 53 s^{-1} is the largest, and that given G = 24 s^{-1} is the second largest, followed by the value given G = 14 s^{-1}, which can also be attributed to the aforementioned explanation. During the flocculation process of type II, the time positions of the individual phases are different for different shear rates. The transitions from type II-phase 1 to type II-phase 2 for G = 14, 24 and 53 s^{-1} occurs at t = 25.72, 18.53 and 14.78 min respectively, whereas type II-phase 3 are reached at t = 75.63, 39.71 and 19.98 min, respectively. The time positions corresponding to these transitions shifted to earlier time points for higher shear rates because the collision frequency function of primary particles/flocs is directly proportional to the shear rate. Moreover, the breakage rate has simply been regarded to be proportional to the 1.5 power of the shear rate in some heuristic models [1,32,52,53,58]. Therefore, the complete process of floc growth, breakage and restructuring progresses more rapidly at higher shear rates. This results in the occurrence of an early time shift in the individual phases of the flocculation process for higher shear rates.

In contrast with the type I and type II flocculation processes, the manner in which the median floc size evolves with time for the shear case of G = 31 s^{-1} in the figure is unique. The size-time curve contains typical characteristics of the type II flocculation development, *i.e.*, attainment of a local peak value at $t^* = 0.73$, and a subsequent decrease in the median size with time ($0.73 < t^* < 2.20$). Corresponding with typical properties of the type I flocculation process, the median size undergoes a slow increase with time ($2.20 < t^* < 6.59$) before finally approaching a steady-state or equilibrium value ($t^* > 6.59$). Compared with the type I and type II processes, one possible heuristic interpretation of this type of flocculation process is depicted below. The flow shear increases the collision frequency of primary particles in the flow and some large, highly branched and loosely bounded flocs are generated, leading to a rapid increase in the median floc size during the early stage of the flocculation process

($0 < t^* < 0.73$). During some time ($0.73 < t^* < 2.20$), these flocs may experience strong structural rearrangements (restructurings) with few breakages when they are exposed to the shear flow (*i.e.*, denser adjustment of floc structure results in a smaller floc size, and the dominance of this restructuring effect over the aggregation effect results in a reduction of the median floc size with time). As the time that the flocs are exposed to the shear flow increases ($2.20 < t^* < 6.59$), the breakage of the floc caused by the shear flow begins to play a noticeable role. However, this breakage effect may not predominate over the aggregation effect because the flocs possess a compact structure, a greater inner bonding strength after the restructuring process, and are more resistant to the shear flow. These traits may cause the median floc size to increase again with flocculation time. After a longer period ($t^* > 6.59$), the steady state (*i.e.*, the median floc size changes with time no more) is approached resulting from a dynamic balance between the aggregation and breakage effects. More evidence for the aforementioned explanation and additionally possible physical mechanisms implied in the aforementioned flocculation process will be worthy of further investigation in future research.

As shown in Figure 4, a steady-state floc size distribution is attained for t^* = 5~6, regardless of the shear rates. Thus, larger shear rates correspond with systems that reach the steady state faster. We also found that the flocculation development for shear rates of 5.36, 9.17, 14, 24, 31, 41 and 53 s^{-1} reached a steady state at 198, 115, 76, 44, 34, 26 and 20 min, respectively.

3.2. Fractal Dimension of the Flocs with Respect to Shear Rate

Figure 5a–c, and d show the D_2, D_1, D_{pf} and AR values of the flocs at steady state with respect to shear conditions of 5.36, 9.17, 14, 24, 31, 41 and 53 s^{-1}. Although the identification of some explicit fitting functions for evaluating the variations of the D_2, D_1 and AR values with respect to shear rates seems nearly impossible, some typical characteristics can be observed by comparing these values in the groups with low shear rates (G = 5.36, 9.17, 14 s^{-1}) and high shear rates (G = 31, 41, 53 s^{-1}). As shown in Figure 5a, the values for D_2 range from 1.72 ± 0.03 to 1.92 ± 0.03 and are similar to the values reported by Gorczyca and Ganczarczyk and De Boer [59,60]. Specifically, the D_2 range increased from 1.73 ± 0.03, 1.72 ± 0.03, and 1.75 ± 0.04 in the low shear group to 1.92 ± 0.03, 1.82 ± 0.02, 1.85 ± 0.02, and 1.81 ± 0.02 under the shear condition of G = 24 s^{-1} and in the high shear group, respectively. This result indicates that the flocs become less elongated under high shear conditions than under low shear conditions due to more breakages and the possible restructurings of the flocs at high shear rates. As shown in Figure 5b, the values of D_1 vary between 1.39 ± 0.02 and 1.63 ± 0.02 and decrease from 1.52 ± 0.02, 1.48 ± 0.02, 1.55 ± 0.02, and 1.63 ± 0.02 in the low shear group with the shear condition of G = 24 s^{-1} to 1.45 ± 0.02, 1.39 ± 0.02, and 1.39 ± 0.02 in the high shear group. This observation implies that the boundary lines of the flocs become tighter and more regular under high shear rates than under low shear rates because more breakups and restructurings occur in the stronger shear environment. The values for D_{pf} (presented in Figure 5c) are from 1.52 ± 0.01 to 1.78 ± 0.02, which is larger than the range of 1.13~1.22 reported by Li and Ganczarczyk, who studied activated sludge floc; a range of 1.25~1.42 was reported in the Canadian province of Saskatchewan [60,61] for suspended solids, and the range of 1.24~1.35 was reported for Ontario streams [62]. In addition, these values decrease with increasing shear rates according to the following function: $D_{pf} = -0.0052G + 1.7894$, with a correlation coefficient of R^2 = 0.84. Thus, a higher shear stress results in flocs with less convoluted and smoother boundaries and

more regular shapes due to breakage and restructuring processes. The *AR* values vary from 1.43 to 1.59 (Figure 5d), and decrease from 1.56, 1.59, 1.53, and 1.51 in the low shear group with the shear condition of $G = 24\ s^{-1}$ to 1.43, 1.47, and 1.48 in the high shear group. This indicates that the shapes of the flocs become more symmetrical at high shear rates than under low shear conditions due to serious breakages and restructurings when they are subject to a strong shear flow, as noted above. A comparative analysis of the behaviors presented here and the experimental/observational results reported by other authors [7,8,27,63] was performed as follows. Using the imaging analysis method, Spicer and Pratsinis [27] studied the time evolution of polystyrene flocs that were destabilized by three concentrations of aluminum sulfate with time (4.3, 10.7, and 32 mg/L) under three shear conditions ($G = 63$, 95, and $129\ s^{-1}$) in a stirred tank and found that the steady state D_{pf} value significantly decreased as the shear rate increased from relative low values ($G = 63$, $95\ s^{-1}$) to larger values ($G = 129\ s^{-1}$) when the aluminum sulfate concentration was 32 mg/L. This finding was attributed to the fact that greater amounts of breakage and restructuring resulted from the increasing shear rate, which resulted in a more compact floc structure. From these experimental results, it can also be observed that the D_{pf} value increased when the aluminum sulfate concentration was 4.3 mg/L and the shear rate increased ($G = 63 \rightarrow 95 \rightarrow 129\ s^{-1}$). However, the D_{pf} value decreased and then increased when the aluminum sulfate concentration was 10.7 mg/L. In both cases, the reasons for these changes were not discussed. Serra and Casamitjana [8] investigated the structures of the flocs during the aggregation and breakage process of latex particles in a Couette-flow shear environment using a video camera and reported no significant changes in the 2-D, 1-D, perimeter-based fractal dimensions or the aspect ratio during aggregation, breakage, and steady-state conditions for three different shear rates ($G = 25$, 32, and $50\ s^{-1}$). This finding implies that no restructuring presented during the complete aggregation and breakage process. During the measurement experiments of sizes and settling velocities of sediment flocs formed in a laboratory flume by un-intrusive miniature video cameras, Manning and Dyer [63] observed that higher levels of turbulent shear stress resulted in the formation of long, thin, "comet like" flocs in the experimental annual flume, while more spherically shaped flocs were produced at lower turbulent shear levels. However, whether this observation was performed at the steady or equilibrium state of flocculation development was not determined in their study. The observational finding of Manning and Dyer could be partially supported by the experimental results of Stone and Krishnappan on the morphology of cohesive sediment flocs formed in an annular experimental flume under steady-state flows of four shear stresses (0.058, 0.121, 0.212, and 0.323 Pa) using a light microscopy technology and an image analysis system [7,63]. Their experimental findings are as follows: (1) the fractal dimension D_{pf} increased from 1.25 ± 0.005 at a shear stress of 0.058 Pa to a maximum of 1.36 ± 0.002 at 0.121 Pa before slightly decreasing to 1.34 ± 0.01 at 0.323 Pa. The first increase of the D_{pf} value from 1.25 ± 0.005 to 1.36 ± 0.002 was attributed to the production of more flocs with irregular boundaries with an increasing shear stress. However, the subsequent minor decrease from 1.36 ± 0.002 to 1.34 ± 0.01 resulted from the floc break-up because the number of particle collisions under the highest shear condition increased. Only the latter behavior agrees with our experimental results, as presented in Figure 5c, which clearly demonstrates the negative dependence of the D_{pf} value on the shear rate, G, over a large range; (2) The fractal dimension D_1 increased gradually from 1.00 ± 0.006 at 0.058 Pa to a maximum value of 1.25 ± 0.003 at 0.325 Pa, which does not agree with our experimental results (Figure 5b); (3) The fractal dimension D_2 increased continuously from 1.35 ± 0.004 at the shear stress of

0.058 Pa to a maximum value of 1.81 ± 0.005 at the shear stress of 0.325 Pa, which corresponded with our results (Figure 5a) in terms of comparing the D_2 values from the low shear group with those from the high shear group. It is evident that the variations of D_2 with respect to different shear stresses in Stone and Krishnappan's study do not support their conclusion that particles became more elongated with increasing shear stresses because an increase in D_2 should correspond with more production of less elongated flocs as the shear stress increases, as explained in Section 2.1 [7].

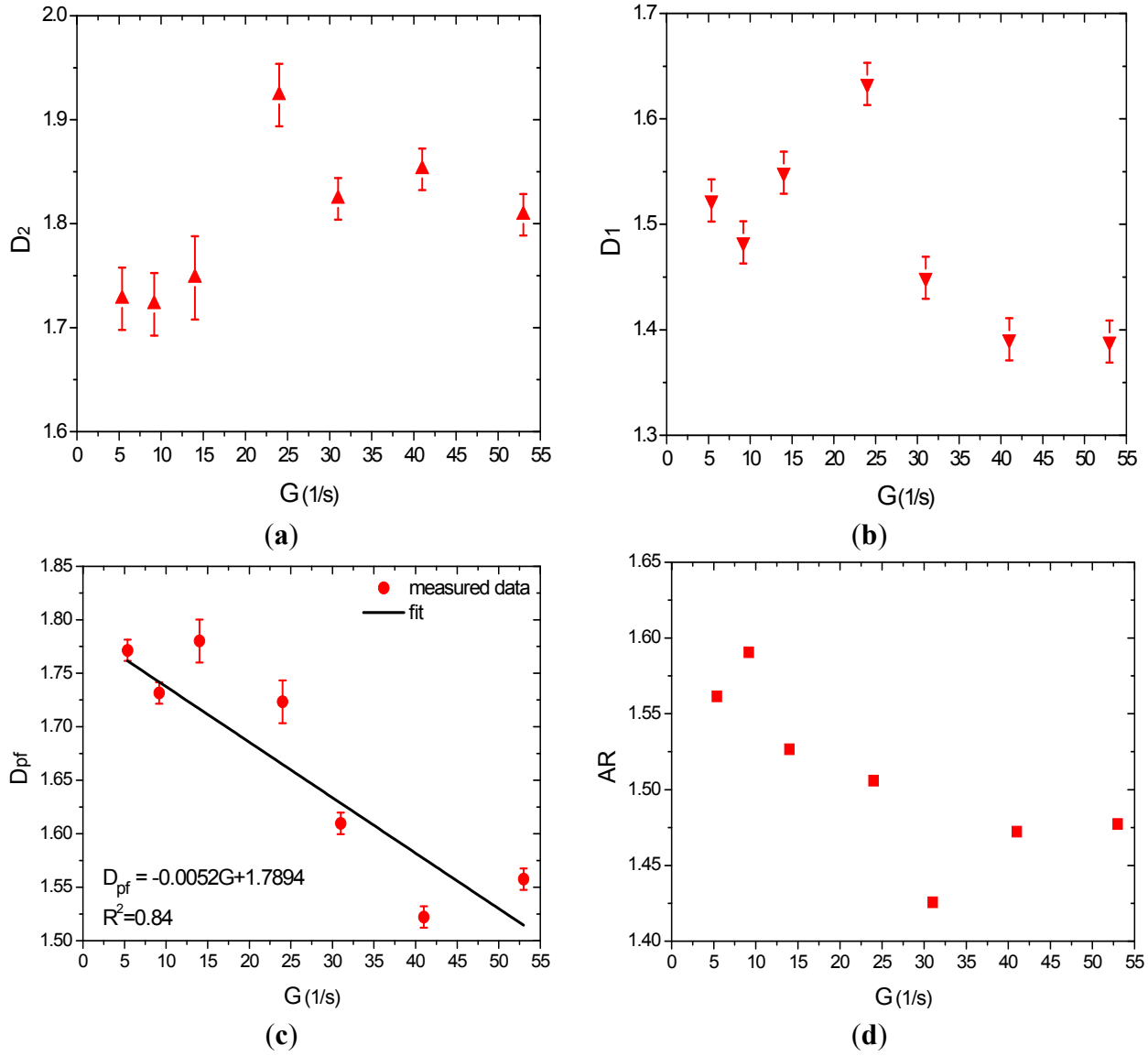

Figure 5. Morphological property parameters of the flocs at steady state with respect to different shear rates at $\phi = 7.87 \times 10^{-5}$ without electrolyte added into the suspension, including 2-D fractal dimension (**a**); 1-D fractal dimension (**b**); perimeter-based fractal dimension (**c**) and aspect ratio (**d**). The error bars in (a–c) show standard deviations of D_2, D_1, and D_{pf} values, respectively.

Considering the important role that the breakage effect plays on the variations of the three fractal dimensions and *AR* with respect to shear rates, as shown in Figure 5, it is important to investigate and examine possible forms of floc breakage. The Kolmogorov micro-scale, η, is a characteristic length of

energy-dissipating eddies during the turbulent flow and is determined using the following expression [1,12,14,27]:

$$\eta = \left(\frac{\nu^3}{\varepsilon} \right)^{\frac{1}{4}} \tag{13}$$

The breakage mechanism of a floc strongly depends on its size relative to the Kolmogorov micro-scale [3,14]. For flocs smaller than the Kolmogorov micro-scale, small primary particles peel off the surface of the "mother" floc due to the viscous shear force (this type of floc breakage has been referred to as surface erosion), whereas large-scale fragmentation is a likely mechanism of floc breakage due to pressure fluctuations in the turbulent flow for flocs larger than the Kolmogorov micro-scale (referred to as large-scale fracture). Table 3 presents a comparison of the Kolmogorov micro-scale and observed maximum floc size with respect to the shear rate. The maximum floc size is always smaller than the Kolmogorov micro-scale at any shear rate; thus, the dominant breakage mechanism for all flocs is surface erosion caused by a viscous shear stress that is larger than the floc strength. For the low shear rate group (G = 5.36, 9.17, and 14 s^{-1}), single primary particles are aggregated into irregular and porous flocs as the shear flow increases their collision frequency. In addition, as the amount of attachment with primary particles increases, the flocs become more highly branched and loosely bound. Thus, it could be inferred that small primary particles distributed on the branches of the floc structure are weakly bound with the main part of the floc and can easily be eroded from the surface of their "mother" floc when the shear stress caused by the shear flow in a Kolmogorov micro-scale eddy surpasses their bonding strengths. In contrast, a high shear rate group (G = 31, 41, and 53 s^{-1}) results in more surface erosions of primary particles from the surface of the "mother" floc. It could be inferred that the "mother" floc becomes less elongated and its boundary becomes less convoluted and more regular in the high shear group than in the low shear group. This result is characterized by an increase in the average value of D_2 from 1.73 ± 0.03 in the low shear group (G = 5.36, 9.17, and 14 s^{-1}) to 1.83 ± 0.02 in the high shear group (G = 31, 41, and 53 s^{-1}), a decrease in the average D_1 value from 1.52 ± 0.02 to 1.41 ± 0.02, a decrease in the average D_{pf} value from 1.76 ± 0.01 to 1.56 ± 0.01, and a decrease in the average AR value from 1.56 to 1.46, respectively, as shown in Figure 5a–d.

Table 3. Comparison of the Kolmogorov micro-scale and maximum floc size with respect to different shear rate, observed during the flocculation process at $\phi = 7.87 \times 10^{-5}$ without electrolyte added into the suspension.

G (s^{-1})	5.36	9.17	14	24	31	41	53
η (μm)	No	330.23	267.26	204.12	179.61	156.17	137.36
Maximum floc size (μm)	No	51.11	134.71	101.05	73.45	64.67	55.13

Note: Caption: the symbol "No" indicates that no Kolmogorov micro-scale eddies exist for the laminar flow.

3.3. Effect of Electrolyte on Floc Fractal Dimension

The aforementioned discussions are based on the background that no electrolyte was added into the suspension. To examine the effect of the electrolyte condition on the morphological properties of the flocs at the steady state of flocculation development, we added calcium chloride ($CaCl_2$) at a

concentration of 0.1 mol/L into the Couette-flow system in this preliminary study. Addition of the electrolyte was done after the releasing process of compressed nitrogen gas. Figure 6a–c, and d show a comparison of the D_2, D_2, D_{pf} and AR values of the flocs under steady-state over a shear rate range (G = 9.17, 14, 24, 31, 41 and 53 s^{-1}) for a case without electrolyte and a case in which 0.1 mol/L $CaCl_2$ was injected into the system. From Figure 6a, it is evident that the addition of $CaCl_2$ resulted in greater D_2 values over a shear rate range, except in the case of G = 31 s^{-1}. As shown in Figure 6b, for half of the cases (G = 9.17, 24, and 31 s^{-1}), the D_1 values decrease as the electrolyte condition was added, and the opposite effect was observed in other cases (G = 14, 41, and 53 s^{-1}). From Figure 6c, the D_{pf} values corresponding to shear rates for the case with electrolyte were always smaller than those without electrolyte, except for the case of G = 41 s^{-1}. As shown in Figure 6d, the addition of electrolyte resulted in decreases in the AR values with different degrees, except for G = 31 s^{-1}. Thus, compared with the case without electrolyte, it can be concluded that the flocs formed in an electrolyte environment become less elongated and more symmetrical. However, six of the 24 shear cases did not support this conclusion. This characteristic is inconsistent with experimental findings of Spicer and Pratsinis regarding the steady-state structures of polystyrene flocs destabilized by three concentrations of aluminum sulfate (4.3, 10.7, and 32 mg/L) in three different shear environments (G = 63, 95, and 129 s^{-1}) in a stirred tank [27], *i.e.*, the D_{pf} value is larger at a high aluminum sulfate concentration (32 mg/L) than in the systems with lower aluminum sulfate concentrations for both shear cases of G = 63, and 95 s^{-1}. This may be owed to the fact that the increased bonding strength within the floc structure could increase the resistance to breakage and lead to a looser steady-state floc structure under higher aluminum sulate concentrations and lower shear conditions. In addition, improving the aluminum sulfate concentration from 4.3 mg/L to 10.7 mg/L in the case of G = 95 s^{-1} and from 10.7 mg/L to 32 mg/L in the largest shear case (G = 129 s^{-1}) resulted in decreases in the D_{pf} values, which is consistent with our results.

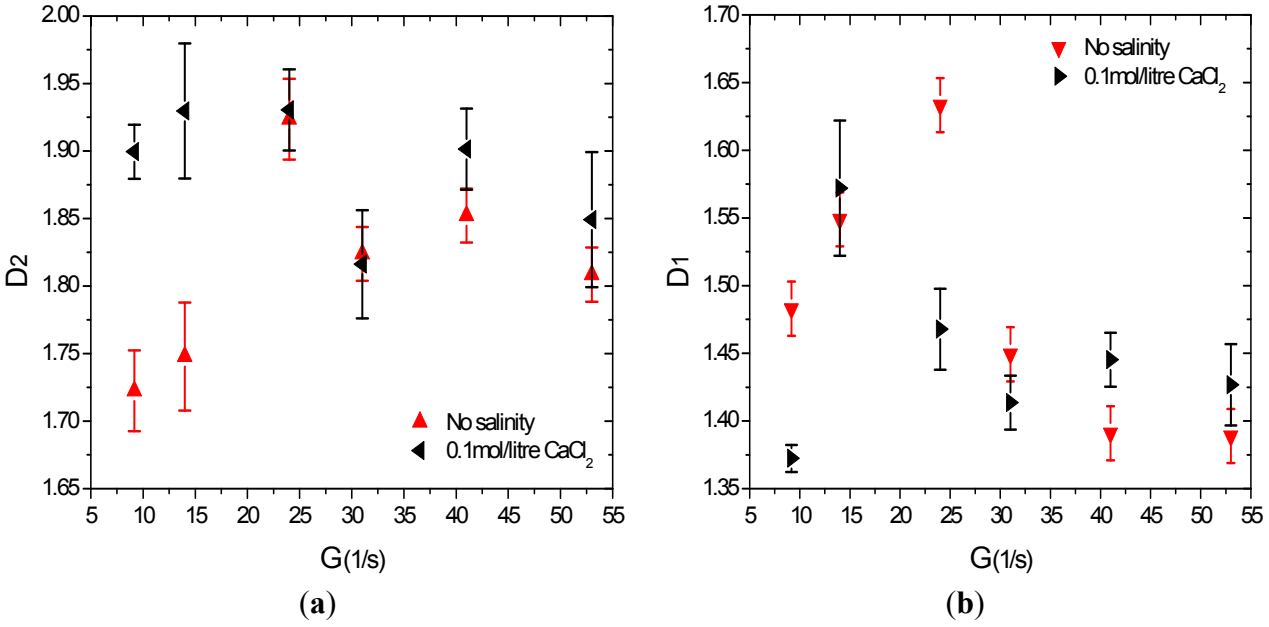

(**a**) (**b**)

Figure 6.*Cont.*

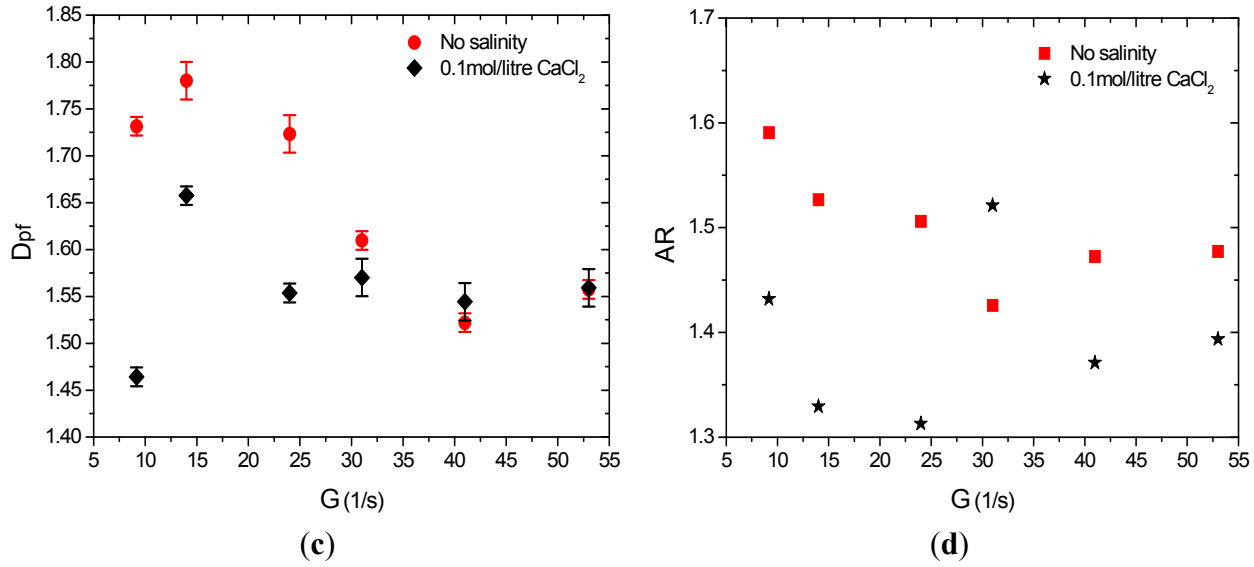

Figure 6. Morphological property parameters of the flocs at steady state over a shear rate range for the non-electrolyte case and the case in which 0.1 mol/L calcium chloride ($CaCl_2$) was added into the suspension at $\phi = 7.87 \times 10^{-5}$, including 2-D fractal dimension (**a**); 1-D fractal dimension (**b**); perimeter-based fractal dimension (**c**) and aspect ratio(**d**). The error bars in (**a**–**c**) show standard deviations of D_2, D_1, and D_{pf} values, respectively.

One possible explanation for the phenomenon presented in our study is that as shown in Section 3.1, the collision efficiency, α, presented in Equation (12) between approaching particles depends on the van der Waals attractive force and the double-layer electrostatic repulsive force between particles for a given shear flow environment. According to the DLVO theory (Deryaguin and Landau (1941) and Verwey and Overbeek (1948), see details in Thomas *et al.*) [3], by describing the combined effects of these forces (see Figure 1 in Thomas *et al.*) [3], the height of the repulsion barrier can be significantly reduced when a certain electrolyte condition is dissolved in the water−sediment mixture, which results in more successful adhesions between primary particles upon collision. Due to increasing attachments between particles, larger, more highly branched and loosely bounded flocs are produced compared with the non-electrolyte shear case. However, these flocs have more porous structures. If it is assumed that the floc strength, σ_T, can be estimated using the following expression, as presented in Tang *et al.* [64]:

$$\sigma_T = 1.1\frac{(1-\varepsilon)}{\varepsilon}\frac{F}{d_{50}^2} \tag{14}$$

where ε is the porosity of the aggregate and F is the bonding force of the van der Waals attractive force and the double-layer repulsive force between primary particles, the inner strengths of those flocs formed in the shear environment with electrolyte can be inferred to be weaker than those in the non-electrolyte environment, because the ε increases significantly despite the larger bonding force F. In this case, the shear flow can result in more severe surface erosions of small primary particles from the floc. Therefore, the floc can become less elongated with a more regular boundary relative to the non-electrolyte condition. More electrolyte types and concentrations will be considered in future experiments, and a detailed analysis of the combined effects of different electrolyte conditions and various shear rates will be conducted in future research.

3.4. Effect of Primary Sediment Concentration on Floc Fractal Dimension

Finally, to explore the effects of initial sediment concentration on the morphological properties of the flocs at the steady state of flocculation process, a change in the initial sediment volumetric concentration ϕ from 7.87×10^{-5} to 1.57×10^{-5} was considered in this preliminary study. Figure 7a–c, and d show a comparison of the D_2, D_1, D_{pf} and AR values under steady-state over three shear rates (G = 24, 31, and 41 s^{-1}) for the case of $\phi = 7.87 \times 10^{-5}$ and for those in another case of $\phi = 1.57 \times 10^{-5}$. As shown in Figure 7a, the D_2 value increases when the initial sediment concentration increases, except when $G = 31$ s^{-1}. The increase in the sediment concentration also resulted in reductions in the D_1, D_{pf} and AR values (Figure 7b–d), except when G = 24 s^{-1}. This result indicates that the flocs formed under high concentration conditions become less elongated with less convoluted and more regular boundary lines relative to environments with low concentrations. However, four of the 12 shear cases did not support this conclusion. The interpretation for this trend is similar to the case in which electrolyte is added, as discussed above. As presented in Equation (12) in Section 3.1, the flocculation rate, k_{ij}, between particles with sizes i and j is directly proportional to the product of their respective number concentrations, n_i and n_j, for a given flocculation system in which the collision efficiency, α, and collision frequency, β_{ij}, between them can be regarded as constants because no electrolyte has been injected and the shear rate is given in this part of the experiment. Therefore, the increase in the initial sediment concentration results in more adhesions between primary particles and causes the formation of more highly branched and loosely bounded floc structures. According to Equation (14), these flocs have weaker bonding strengths because their porosity coefficients, ε, are larger, and the F value remains unchanged. Thus, the flocs experience larger extents of surface erosion due to the flow shear when compared with the case in which a low initial sediment concentration is used, which results in the productions of less elongated and more regular flocs. More initial sediment concentrations and more shear rate conditions will be investigated in future experiments.

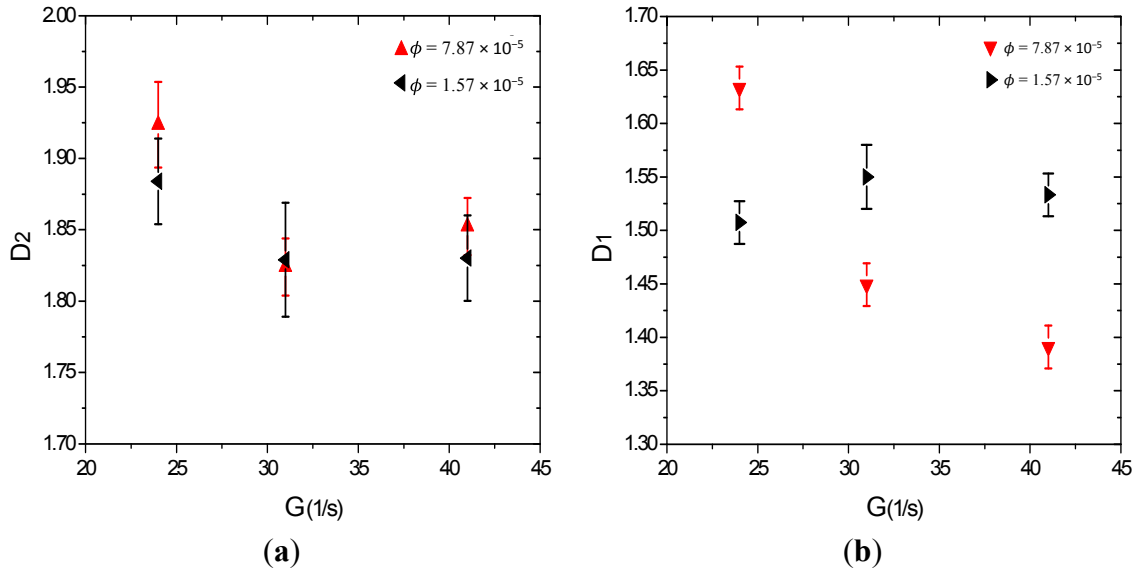

Figure 7. *Cont.*

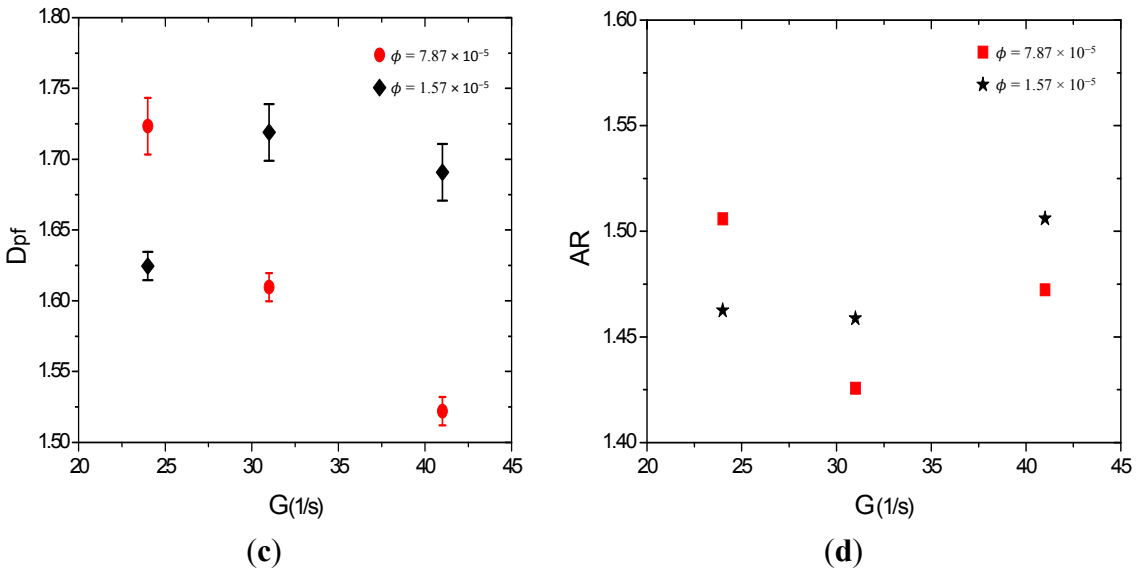

(c) **(d)**

Figure 7. Morphological property parameters of the flocs at steady state with respect to different shear rates for the case in which the primary sediment concentration is 7.87×10^{-5} and the other case where the concentration is 1.57×10^{-5} without electrolyte added into the suspension, including 2-D fractal dimension (**a**); 1-D fractal dimension (**b**); perimeter-based fractal dimension (**c**); and aspect ratio (**d**). The error bars in (**a**–**c**) show standard deviations of D_2, D_1, and D_{pf} values, respectively.

4. Conclusions

In this study, fractal dimensions of cohesive sediment flocs at the steady state of flocculation development under seven flow conditions were studied. The experimental results lead to the following two conclusions:

(1) With increasing shear stresses, the flocs become less elongated and less convoluted, and their boundary lines get tighter and more regular, caused by more breakages and possible restructurings of the flocs at high shear conditions.

(2) As the electrolyte is added and initial sediment concentration goes up, the flocs become less elongated and more symmetrical, and their boundaries become less convoluted and simpler.

Acknowledgments

This work is jointly supported by the National Natural Science Foundation of China (No.: 51279006, 51479003), the Fundamental Research Funds for the Central Universities in China (No.: 2013NT50) and the Project Sponsored by the Scientific Research Foundation for the Returned Overseas Chinese Scholars, State Education Ministry. The first author would like to express his deepest gratitude to Professor Tie-sheng Yang, who retired from the Department of Hydraulic Engineering of Tsinghua University in China, for his careful guidance during the master's research. We would like to express the gratitude to the editor and three anonymous reviewers for their comments and suggestions. Argonne National Laboratory's work was supported by the U.S. Department of Energy, Office of Science, under contract DE-AC02-06CH11357.

Author Contributions

Zhongfan Zhu and Hongrui Wang carried out the experimental work and prepared the manuscript. Jingshan Yu and Jie Dou analysed the results and contributed to the development and editing of the manuscript. Cheng Wang discussed some experimental results and made a contribution to the revision of the manuscript.

Conflicts of Interest

The authors declare no conflicts of interest.

References

1. Winterwerp, J.C. A simple model for turbulence induced flocculation of cohesive sediment. *J. Hydraul. Res.* **1998**, *36*, 309–326.
2. Kranenburg, C. Effects of floc strength on viscosity and deposition of cohesive sediment suspensions. *Cont. Shelf Res.* **1999**, *19*, 1665–1680.
3. Thomas, D.; Judd, S.; Fawcett, N. Flocculation modelling: A review. *Water Res.* **1999**, *33*, 1579–1592.
4. Xu, F.; Wang, D.-P.; Riemer, N. Modeling flocculation processes of fine-grained particles using a size-resolved method: Comparison with published laboratory experiments. *Cont. Shelf Res.* **2008**, *28*, 2668–2677.
5. Dyer, K. Sediment processes in estuaries: Future research requirements. *J. Geophys. Res. Oceans 1978–2012* **1989**, *94*, 14327–14339.
6. Mandelbrot, B.B. *The Fractal Geometry of Nature*; William H. Freeman: New York, NY, USA, 1983.
7. Stone, M.; Krishnappan, B. Floc morphology and size distributions of cohesive sediment in steady-state flow. *Water Res.* **2003**, *37*, 2739–2747.
8. Serra, T.; Casamitjana, X. Structure of the aggregates during the process of aggregation and breakup under a shear flow. *J.Colloid Interface Sci.* **1998**, *206*, 505–511.
9. Bubakova, P.; Pivokonsky, M.; Filip, P. Effect of shear rate on aggregate size and structure in the process of aggregation and at steady state. *Powder Technol.* **2013**, *235*, 540–549.
10. Oles, V. Shear-induced aggregation and breakup of polystyrene latex particles. *J. Colloid Interface Sci.* **1992**, *154*, 351–358.
11. Spicer, P.T.; Keller, W.; Pratsinis, S.E. The effect of impeller type on floc size and structure during shear-induced flocculation. *J. Colloid Interface Sci.* **1996**, *184*, 112–122.
12. Serra, T.; Colomer, J.; Casamitjana, X. Aggregation and breakup of particles in a shear flow. *J. Colloid Interface Sci.* **1997**, *187*, 466–473.
13. Flesch, J.C.; Spicer, P.T.; Pratsinis, S.E. Laminar and turbulent shear—Induced flocculation of fractal aggregates. *AIChE J.* **1999**, *45*, 1114–1124.
14. Biggs, C.; Lant, P. Activated sludge flocculation: On-line determination of floc size and the effect of shear. *Water Res.* **2000**, *34*, 2542–2550.
15. Soos, M.; Wang, L.; Fox, R.; Sefcik, J.; Morbidelli, M. Population balance modeling of aggregation and breakage in turbulent taylor–couette flow. *J. Colloid Interface Sci.* **2007**, *307*, 433–446.

16. Ehrl, L.; Soos, M.; Morbidelli, M. Dependence of aggregate strength, structure, and light scattering properties on primary particle size under turbulent conditions in stirred tank. *Langmuir* **2008**, *24*, 3070–3081.
17. Ehrl, L.; Soos, M.; Morbidelli, M.; Bäbler, M.U. Dependence of initial cluster aggregation kinetics on shear rate for particles of different sizes under turbulence. *AIChE J.* **2009**, *55*, 3076–3087.
18. Ehrl, L.; Soos, M.; Wu, H.; Morbidelli, M. Effect of flow field heterogeneity in coagulators on aggregate size and structure. *AIChE J.* **2010**, *56*, 2573–2587.
19. Keyvani, A.; Strom, K. Influence of cycles of high and low turbulent shear on the growth rate and equilibrium size of mud flocs. *Mar. Geol.* **2014**, *354*, 1–14.
20. Selomulya, C.; Bushell, G.; Amal, R.; Waite, T. Understanding the role of restructuring in flocculation: The application of a population balance model. *Chem. Eng. Sci.* **2003**, *58*, 327–338.
21. Williams, R.; Peng, S.; Naylor, A. In situ measurement of particle aggregation and breakage kinetics in a concentrated suspension. *Powder Technol.* **1992**, *73*, 75–83.
22. Selomulya, C.; Amal, R.; Bushell, G.; Waite, T.D. Evidence of shear rate dependence on restructuring and breakup of latex aggregates. *J. Colloid Interface Sci.* **2001**, *236*, 67–77.
23. Hopkins, D.C.; Ducoste, J.J. Characterizing flocculation under heterogeneous turbulence. *J. Colloid Interface Sci.* **2003**, *264*, 184–194.
24. Rahmani, N.H.; Masliyah, J.H.; Dabros, T. Characterization of asphaltenes aggregation and fragmentation in a shear field. *AIChE J.* **2003**, *49*, 1645–1655.
25. Logan, B.E.; Kilps, J.R. Fractal dimensions of aggregates formed in different fluid mechanical environments. *Water Res.* **1995**, *29*, 443–453.
26. Jiang, Q.; Logan, B.E. Fractal dimensions of aggregates determined from steady-state size distributions. *Environ. Sci. Technol.* **1991**, *25*, 2031–2038.
27. Spicer, P.T.; Pratsinis, S.E. Shear-induced flocculation: The evolution of floc structure and the shape of the size distribution at steady state. *Water Res.* **1996**, *30*, 1049–1056.
28. Mandelbrot, B.B.; Passoja, D.E.; Paullay, A.J. Fractal character of fracture surfaces of metals. *Nature* **1984**, *308*, 721–722.
29. Serra, T.; Colomer, J.; Logan, B.E. Efficiency of different shear devices on flocculation. *Water Res.* **2008**, *42*, 1113–1121.
30. Bouyer, D.; Line, A.; Cockx, A.; Do-Quang, Z. Experimental analysis of floc size distribution and hydrodynamics in a jar-test. *Chem. Eng. Res. Des.* **2001**, *79*, 1017–1024.
31. Colomer, J.; Peters, F.; Marrasé, C. Experimental analysis of coagulation of particles under low-shear flow. *Water Res.* **2005**, *39*, 2994–3000.
32. Winterwerp, J. On the flocculation and settling velocity of estuarine mud. *Cont. Shelf Res.* **2002**, *22*, 1339–1360.
33. Camp, T.R.; Stein, P.C. Velocity gradients and internal work in fluid motion. *J. Boston Soc. Civil Eng.* **1943**, *85*, 219–237.
34. Hinze, J.O. *Turbulence*, 2nd ed.; McGraw-Hill: New York, NY, USA, 1975.
35. Zhu, Z. The Investigation on Phase Transition and the Influence of Shear on the Flocculation of Cohesive Sediment. Master's Thesis, Tsinghua University, Beijing, China, 2009.
36. Lazier, J.; Mann, K. Turbulence and the diffusive layers around small organisms. *Deep Sea Res. Part A. Oceanogr. Res. Pap.* **1989**, *36*, 1721–1733.

37. Bowen, J.D.; Stolzenbach, K.D.; Chisholm, S.W. Simulating bacterial clustering around phytoplankton cells in a turbulent ocean. *Limnol. Oceanogr.* **1993**, *38*, 36–51.
38. Kumar, R.G.; Strom, K.B.; Keyvani, A. Floc properties and settling velocity of san jacinto estuary mud under variable shear and salinity conditions. *Cont. Shelf Res.* **2010**, *30*, 2067–2081.
39. Kiørboe, T.; Saiz, E. Planktivorous feeding in calm and turbulent environments, with emphasis on copepods. *Mar. Ecol. Prog. Ser.* **1995**, *122*, 135–145.
40. Lick, W.; Lick, J. Aggregation and disaggregation of fine-grained lake sediments. *J. Great Lakes Res.* **1988**, *14*, 514–523.
41. Burban, P.Y.; Lick, W.; Lick, J. The flocculation of fine—Grained sediments in estuarine waters. *J. Geophys. Res. Ocean. 1978–2012* **1989**, *94*, 8323–8330.
42. Estrada, M.; Berdalet, E. Phytoplankton in a turbulent world. *Sci. Mar.* **1997**, *61*, 125–140.
43. Crittenden, J.C.; Trussell, R.R.; Hand, D.W.; Howe, K.J.; Tchobanoglous, G. *Mwh's Water Treatment: Principles and Design*, 2nd ed.; John Wiley & Sons: Hoboken, NJ, USA, 2005.
44. Chandrasekhar, S. *Hydrodynamic and Hydromagnetic Stability*; Clarendon Press: Oxford, UK, 1961; Volume 196.
45. Maggi, F. Variable fractal dimension: A major control for floc structure and flocculation kinematics of suspended cohesive sediment. *J. Geophys. Res. Ocean. 1978–2012* **2007**, *112*, doi:10.1029/2006JC003951.
46. Maggi, F.; Mietta, F.; Winterwerp, J. Effect of variable fractal dimension on the floc size distribution of suspended cohesive sediment. *J. Hydrol.* **2007**, *343*, 43–55.
47. Tambo, N.; Watanabe, Y. Physical aspect of flocculation process—I: Fundamental treatise. *Water Res.* **1979**, *13*, 429–439.
48. Francois, R. Growth kinetics of hydroxide flocs. *J. Am. Water Works Assoc.* **1988**, *80*, 92–96.
49. Gibbs, R.J.; Konwar, L.N. Effect of pipetting on mineral flocs. *Environ. Sci. Technol.* **1982**, *16*, 119–121.
50. Lick, W.; Huang, H.; Jepsen, R. Flocculation of fine—Grained sediments due to differential settling. *J. Geophys. Res. Ocean. 1978–2012* **1993**, *98*, 10279–10288.
51. Stolzenbach, K.D.; Elimelech, M. The effect of particle density on collisions between sinking particles: Implications for particle aggregation in the ocean. *Deep Sea Res. Part I Oceanogr. Res. Pap.* **1994**, *41*, 469–483.
52. Son, M.; Hsu, T.-J. Flocculation model of cohesive sediment using variable fractal dimension. *Environ. Fluid Mech.* **2008**, *8*, 55–71.
53. Son, M.; Hsu, T.-J. The effect of variable yield strength and variable fractal dimension on flocculation of cohesive sediment. *Water Res.* **2009**, *43*, 3582–3592.
54. Smoluchowski, M. Mathematical theory of the kinetics of the coagulation of colloidal solutions. *Z. Phys. Chem*. **1917**, *92*, 129.
55. Prat, O.P.; Ducoste, J.J. Modeling spatial distribution of floc size in turbulent processes using the quadrature method of moment and computational fluid dynamics. *Chem. Eng. Sci.* **2006**, *61*, 75–86.
56. Kusters, K.A.; Wijers, J.G.; Thoenes, D. Aggregation kinetics of small particles in agitated vessels. *Chem. Eng. Sci.* **1997**, *52*, 107–121.
57. Francois, R. Strength of aluminium hydroxide flocs. *Water Res.* **1987**, *21*, 1023–1030.

58. Winterwerp, J.; Manning, A.; Martens, C.; de Mulder, T.; Vanlede, J. A heuristic formula for turbulence-induced flocculation of cohesive sediment. *Estuar. Coast. Shelf Sci.* **2006**, *68*, 195–207.
59. Gorczyca, B.; Ganczarczyk, J. Image analysis of alum coagulated mineral suspensions. *Environ. Technol.* **1996**, *17*, 1361–1369.
60. De Boer, D.H. An evaluation of fractal dimensions to quantify changes in the morphology of fluvial suspended sediment particles during baseflow conditions. *Hydrol. Process.* **1997**, *11*, 415–426.
61. Li, D.H.; Ganczarczyk, J. Fractal geometry of particle aggregates generated in water and wastewater treatment processes. *Environ. Sci. Technol.* **1989**, *23*, 1385–1389.
62. De Boer, D.H.; Stone, M. Fractal dimensions of suspended solids in streams: Comparison of sampling and analysis techniques. *Hydrol. Process.* **1999**, *13*, 239–254.
63. Manning, A.; Dyer, K. A laboratory examination of floc characteristics with regard to turbulent shearing. *Mar. Geol.* **1999**, *160*, 147–170.
64. Tang, S.; Ma, Y.; Shiu, C. Modelling the mechanical strength of fractal aggregates. *Colloids Surf. A Physicochem. Eng. Asp.* **2001**, *180*, 7–16.